Title
Low-voltage fast seizures in humans begin with increased interneuron firing.

Journal
Annals of neurology, 84(4)

ISSN
0364-5134

Authors
Elahian, Bahareh
Lado, Nathan E
Mankin, Emily
et al.

Publication Date
2018-10-01

DOI
10.1002/ana.25325

Peer reviewed

HHS Public Access

Author manuscript

Ann Neurol. Author manuscript; available in PMC 2019 October 25.

Published in final edited form as:

Ann Neurol. 2018 October ; 84(4): 588–600. doi:10.1002/ana.25325.

Low-Voltage Fast Seizures in Humans Begin with Increased Interneuron Firing

Bahareh Elahian, PhD[1,2,3], **Nathan E. Lado, BA**[1,2], **Emily Mankin, PhD**[4], **Sitaram Vangala, MS**[5], **Amrit Misra, MD, PhD**[6], **Karen Moxon, PhD**[7], **Itzhak Fried, MD, PhD**[4], **Ashwini Sharan, MD**[8], **Mohammed Yeasin, PhD**[3], **Richard Staba, PhD**[9], **Anatol Bragin, PhD**[9], **Massimo Avoli, MD, PhD**[10,11,12], **Michael R. Sperling, MD**[2], **Jerome Engel Jr, MD, PhD**[13,14], **Shennan A. Weiss, MD, PhD**[1,2]

[1]Department of Neuroscience, Thomas Jefferson University, Philadelphia, PA;

[2]Department of Neurology, Thomas Jefferson University, Philadelphia, PA;

[3]Department of Electrical and Computer Engineering, University of Memphis, Memphis, TN;

[4]Department of Neurosurgery, David Geffen School of Medicine at UCLA, Los Angeles, CA;

[5]Department of Medicine, Statistics Core, David Geffen School of Medicine at UCLA, Los Angeles, CA;

[6]Department of Neurology, Massachusetts General Hospital, Boston, MA;

[7]Department of Biomedical Engineering, Science, and Health Systems, Drexel University, Philadelphia, PA;

[8]Department of Neurosurgery, Thomas Jefferson University, Philadelphia, PA;

[9]Department of Neurology, David Geffen School of Medicine at UCLA, Los Angeles, CA;

[10]Department of Neurology and Neurosurgery, McGill University, Montreal, Quebec, Canada;

[11]Department of Physiology, McGill University, Montreal, Quebec, Canada;

[12]Montreal Neurological Institute, McGill University, Montreal, Quebec, Canada;

[13]Department of Neurobiology, David Geffen School of Medicine at UCLA, Los Angeles, CA;

[14]Department of Psychiatry and Biobehavioral Sciences, Brain Research Institute, David Geffen School of Medicine at UCLA, Los Angeles, CA

Abstract

Objective: Intracellular recordings from cells in entorhinal cortex tissue slices show that low-voltage fast (LVF) onset seizures are generated by inhibitory events. Here, we determined whether

Address correspondence to Dr Weiss, 901 Walnut St, Suite 400, Philadelphia, PA 19107. Shennan.Weiss@jefferson.edu.

Author Contributions

S.A.W. and B.E. contributed to conception and design of the study; E.M., A.M., K.M., I.F., A.S., and R.S. contributed to acquisition of the data; B.E., N.E.L., S.V., and S.A.W. contributed to analysis of the data; all authors contributed to drafting the text and preparing the figures.

Potential Conflicts of Interest

S.A.W. is a founder of Fastwave, an EEG software manufacturer.

increased firing of interneurons occurs at the onset of spontaneous mesial–temporal LVF seizures recorded in patients.

Methods: The seizure onset zone (SOZ) was identified using visual inspection of the intracranial electroencephalogram. We used wavelet clustering and temporal autocorrelations to characterize changes in single-unit activity during the onset of LVF seizures recorded from microelectrodes in mesial–temporal structures. Action potentials generated by principal neurons and interneurons (ie, putative excitatory and inhibitory neurons) were distinguished using waveform morphology and K-means clustering.

Results: From a total of 200 implanted microelectrodes in 9 patients during 13 seizures, we isolated 202 single units; 140 (69.3%) of these units were located in the SOZ, and 40 (28.57%) of them were classified as inhibitory. The wave-forms of both excitatory and inhibitory units remained stable during the LVF epoch ($p > > 0.05$). In the mesial–temporal SOZ, inhibitory interneurons increased their firing rate during LVF seizure onset ($p < 0.01$). Excitatory neuron firing rates peaked 10 seconds after the inhibitory neurons ($p < 0.01$). During LVF spread to the contralateral mesial temporal lobe, an increase in inhibitory neuron firing rate was also observed ($p < 0.01$).

Interpretation: Our results suggest that seizure generation and spread during spontaneous mesial–temporal LVF onset events in humans may result from increased inhibitory neuron firing that spawns a subsequent increase in excitatory neuron firing and seizure evolution.

In focal epileptic disorders, it is commonly believed that transition from a preictal to an ictal state is due to an excessive synchronization of excitatory neuronal networks caused by the weakening of synaptic inhibition (see for review: Ayala et al,[1] Trevelyan et al[2]. However, this concept, although “logically obvious,” is not supported by any firm experimental evidence. Rather, studies performed in acute seizure models and chronic models of epilepsy show that focal seizures, particularly those that begin with low-voltage fast (LVF) activity, are paradoxically initiated by synchronous inhibitory cell spike firing (see for review: Avoli et al,[3] de Curtis and Avoli[4]. LVF seizures, which are often heralded by an electroencephalographic (EEG) spike and immediately followed by beta-gamma frequency activity, have a regional onset and frequently involve mesial and lateral temporal lobe structures.[5–7] In addition, LVF onset seizures in patients with mesial–temporal lobe epilepsy are associated with distinct neuroanatomical changes such as atypical patterns of hippocampal sclerosis (HS), and lower likelihood for seizure freedom than patients with classical HS and hypersynchronous onset seizures, presumably due to the more extensive temporal and extratemporal epileptogenic zone.[8,9]

Findings obtained in vitro from entorhinal cortex and hippocampal tissue slices and from isolated guinea pig preparation show that 4-aminopyridine or bicuculline application induces LVF seizurelike discharges that coincide with sustained interneuron discharges and robust inhibitory postsynaptic events in principal (glutamatergic) neurons.[4,10–14] In line with these findings, optogenetic stimulation of parvalbumin- or somatostatin-positive interneurons can initiate ictallike LVF onset events similar to those occurring spontaneously.[15–17] Experimentally, LVF onset seizures are also recorded in status epilepticus-induced models of mesial–temporal lobe epilepsy. Single-unit recordings obtained in vivo from the

hippocampus of these epileptic animals have shown that seizure onset correlates with an arrest of principal neuron firing along with increased interneuron discharge.[18–23] Because the specific imbalance between excitation and inhibition at LVF onset has only been observed in pharmacological and optogenetic models, the relevance to spontaneous LVF seizure genesis in humans with epilepsy remains unclear. Limited prior in vivo extracellular recordings of action potentials during spontaneous seizures with LVF onset in humans have demonstrated both highly heterogeneous ensemble activity[24,25] and suppressed firing followed by a slowly propagating wave of increased neuronal firing.[26] In the current study, we analyzed wide bandwidth recordings from microelectrodes positioned in mesial–temporal structures of presurgical patients with drug-resistant focal seizures. We used single-unit analysis to discriminate action potentials generated by putative excitatory from inhibitory cells, and evaluated cell type-specific firing during spontaneous LVF onset seizures.

Patients and Methods

Subjects

We retrospectively analyzed data obtained from 7 patients at University of California, Los Angeles (UCLA) and 2 patients at Thomas Jefferson University (TJU) during 13 spontaneous seizures at the time of intracranial monitoring using custom[27] or commercial Behnke-Fried combined macro- and microdepth electrodes (Ad-Tech, Racine, WI), respectively. The electrodes were localized to anatomical regions as described previously.[28] The study was independently approved by the institutional review boards of UCLA and TJU, and all patients provided informed consent before participating in this research. Only patients with LVF onset seizures in the mesial–temporal lobe were included in the study. LVF onset was confirmed by intracranial EEG (iEEG) review (S.A.W. and R.S.).

Recordings

Wide bandwidth (0.001–8 kHz) iEEG and local field potentials (LFPs) were recorded from macro- and microelectrode contacts, respectively (40k samples/sec; gain × 10,000) and amplified using an Atlas system (Neuralynx, Bozeman, MT). In some experiments, wide bandwidth (0.001–6kHz) LFPs were recorded from microelectrodes using either a Cheetah (Neuralynx) or a NeuroPort recording system (Blackrock, Salt Lake City, UT; 28–30kAmp/s; gain x 10,000). In these latter experiments, wide bandwidth iEEG was recorded using a Stellate (XLTEK, San Diego, CA) or a 128-channel NK 1200 long-term monitoring system (Nihon-Kohden America, Foothill Ranch, CA).

Data Analysis

Extracting Seizures from Continuous LFP Recordings.—Each seizure and the time of seizure onset were detected in the continuous LFP recording using custom software written in MATLAB (MathWorks, Natick, MA). For each seizure, a segment or clip of the LFP recording was generated; it contained the seizure onset and the entirety of the LVF onset pattern. In all but 1 seizure, the clip included at least a 3-minute preictal epoch. Synchronized LFP-iEEG recordings from both the microelectrodes and clinical macroelectrodes were available for 6 of the 13 seizures.

Defining Seizure Onset Patterns Using LFP Recordings.—The seizure onset zone (SOZ) and non-SOZ regions were identified on the basis of visual inspection of the iEEG by a board-certified clinician. The EEG seizure onset pattern (LVF, hypersynchronous, repetitive spike and wave) and the time of seizure onset were established on the basis of visual inspection of the LFP by S.A.W. and B.E. (cf Perucca et al,[7] Weiss et al[29]. We used criteria of clearly visible rhythmic activity > 13Hz that was between 10 and 40 μV (Perucca et al[7]. The time of LVF onset and offset was determined by visual inspection of the LFP recordings in MATLAB and using normalized spectrograms generated using the short-time Fourier transform function in MATLAB by S.A.W. and B.E.

Single- and Multiunit Action Potential Sorting and Quality Control.—We visually inspected each LFP clip before and after bandpass (300–3,000Hz) filtering using a 1,000th order symmetric finite impulse response digital filter. If the recordings contained neuronal action potentials and an absence of high-frequency artifact, then we used the unsupervised spike detection and sorting algorithm Wave_clus[30] to characterize single-unit activity (SUA) in the LFP. Following action potential sorting, we quantified the number of false action potentials that violated the relative and absolute refractory periods of 3 and 1 milliseconds, respectively.[31] In the case of refractory period violations, the action potential sorting was repeated using different parameters. Extracellular unit action potentials were identified using a threshold of 5.92 × median of the absolute deviation of the signal.[32] Following spike sorting, the binary vectors of SUA and multiunit activity (MUA) were downsampled to 10kHz (ie, 0.1-millisecond bins).

Single-Unit Characterization.—We analyzed the mean action potential waveform of each single unit and extracted the peak amplitude asymmetry, trough to the following peak, and half width of half amplitude of the action potential. Using these features, excitatory and inhibitory neurons were differentiated on the basis of K-mean clustering.[33] Before comparing mean firing rates between putative inhibitory and excitatory neurons, spike trains were smoothed with a 100millisecond Gaussian kernel and then downsampled to 100Hz. A long-duration kernel was used because of the relatively sparse unit firing. To characterize the firing properties of the putative excitatory and inhibitory neurons over longer epochs, we utilized 45-to 60-minute peri-ictal LFP recordings from the SOZ that were available for a subset of the patients (487, 488, 489). We first removed the ictal portions of the recording, and then identified and characterized the SUA to generate binary vectors of the action potentials in 1-millisecond bins. The mean interspike interval (ISI) was computed with a resolution of 1 millisecond and a maximal time interval of 10 seconds, using 3 distinct epochs consisting of 5 to 40 minutes of baseline, 5 minutes of preictal, and 5 to 40 minutes of postictal activity. The precise duration of these epochs depended on the time of occurrence of the seizure in the original 45- to 60-minute recording.

Changes in Waveform during LVF Epoch.—To determine whether the waveforms of the putative excitatory and inhibitory neurons, and multiunit action potentials, were stable during the LVF epoch, we normalized each wave-form and calculated the coefficients and score of the principal components of all the action potential waveforms during the preictal epoch. We applied these same coefficients to the action potential waveforms that occurred

during the LVF epoch to derive scores for the action potentials. We next assessed the Mahalanobis distance between the centroids identified using the scores of the first and second component of the pre- and post-LVF action potentials.[34] The critical value for a significant difference in the Mahalanobis distance was derived using a chi-squared distribution with 1 degree of freedom and used to define a change in waveform morphology during the LVF epoch.

Phase Relationships between Action Potentials and LVF Oscillations.—The instantaneous phase of each LFP during the LVF epoch was calculated by applying a Hilbert transform to the bandpass-filtered LFP recording in the high LVF band (20–30Hz). The Hilbert transform is defined as $Y_{[t]} = \mathrm{H}\left(\mathrm{X}_{[t]}\right) = \frac{1}{\pi}\int_{-\infty}^{\infty}\frac{x[\tau]}{t-\tau}d\tau$ and results in the analytic signal $z_{[n]} = a_{[n]}\exp(i\,\theta_{[n]})$, where $a_{[n]}$ is the instantaneous amplitude of $Y_{[t]}$ and $\theta_{[n]}$ is the instantaneous phase. The phase angle of each action potential with respect to the LVF band (20–30Hz) was determined by evaluating the instantaneous phase vector $\theta_{[n]}$ at the time at which each binarized action potential occurred. The first trigonometric moment of these phase angles (ϕ_{spike}) was derived using the equation $\mathrm{m}' = \sum exp^{i\phi_{spike}} = \mathrm{R}exp^{i\theta}$.[35] Rayleigh Z test for circular uniformity was calculated as $Z = nR^2$. The probability that the null hypothesis holds was estimated as $p = exp^{-Z}$.[36]

Statistical Analysis.—To determine whether single units increase firing rates prior to or during the LVF epoch, combined local regression (LOESS)–linear mixed regression models were used. The purpose of employing the LOESS models was to estimate the timing of the peak firing rate in each series by first reducing variability. The linear mixed models were based on the raw firing rates and were used to determine significant changes. LOESS was used to generate a nonparametrically smoothed firing rate profile prior to and in response to seizure onset, with a smooth parameter of 0.3. In one set of linear mixed models, observations were clustered by patient using patient random effects, and in the other they were clustered by electrode using electrode-within-patient nested random effects. For the 6 main analyses, the following subsamples were used: (1) inhibitory, entorhinal cortex, SOZ; (2) excitatory, entorhinal cortex, SOZ; (3) excitatory, hippocampus/amygdala, SOZ; (4) inhibitory SOZ; (5) inhibitory, non-SOZ; and (6) excitatory, SOZ. Fixed effects included period relative to seizure onset (baseline [−100…−50 seconds prior to LVF onset], preictal [−50…0 seconds prior to LVF onset], and ictal [following LVF onset]), and models were fitted with and without a linear time-within-period effect. For sites of spread, LVF onset referred to the appearance of LVF activity at that microelectrode recording site. Comparisons of mean firing rate between periods relative to seizure onset were performed using model contrasts. Probability values less than 0.05 were considered statistically significant. All analyses were performed using SAS v9.4 (SAS Institute, Cary, NC). To find the peak time of highest firing rate, we used the local regression method to generate a single curve, find the maximum value of the curve, and get the time corresponding to it on the curve after LOESS smoothing.

Results

Description of Patients and Seizures

We analyzed LFPs and SUA recorded from 200 micro-electrodes implanted in 9 patients during 13 spontaneous focal seizures with impaired awareness (Table). Of the 9 patients, 7 were diagnosed with mesial temporal lobe epilepsy (MTLE) and seizures began in mesial temporal structures; 1 patient had mesial temporal and frontal lobe seizures, and the other had bilateral mesial temporal seizures. Of the 7 patients with unilateral MTLE, 5 had anterior temporal lobe resection and 3 became seizure-free. Only 1 of them had hippocampal sclerosis. The other 2 patients (462, TJ041) had MTLE "plus" and the SOZ included mesial–temporal lobe and temporal neocortex. In these latter patients, the seizures propagated in <1 second to the ipsilateral mesial–temporal lobe; 1 had an anterior temporal lobe resection and the other had a lateral temporal lobe resection that spared the hippocampus. Both patients continued to have seizures, although seizure frequency and severity were decreased. All the seizures recorded by the microelectrode began with an LVF EEG pattern (Fig 1A),[5] and 7 of the 13 seizures were heralded by a single EEG spike or a polyspike prior to LVF activity (see Fig 1A).

Isolation and Characterization of Single Units

To distinguish putative excitatory from inhibitory units, we measured the peak amplitude asymmetry, half width, and trough to peak of the mean spike waveform for each single unit (see Fig $1C_2$). Interneurons that are putatively inhibitory neurons are known to exhibit narrower spike waveforms (ie, half width), and a higher asymmetry index reflecting a different time course of repolarization as compared to principal, that is, putative excitatory neurons.[37] Plotting these spike waveform features produced 2 distinct clusters. The cluster containing spike waveforms with a shorter half width, shorter trough to peak duration, and larger peak amplitude asymmetry were classified as putative inhibitory interneurons (see Fig 1B, C), whereas the second cluster of spike waveforms was classified as putative excitatory principal cells.[14]

Overall, we identified 100 excitatory neurons and 40 inhibitory neurons in the mesial–temporal SOZ using waveform morphology criteria. We also identified 49 excitatory neurons, and 13 inhibitory mesial–temporal neurons contralateral to the SOZ. For patient 462, who presented with MTLE + and a mesial–temporal and neocortical seizure onset, we considered the ipsilateral mesial–temporal structures as part of the SOZ because they represented the site of rapid propagation (<1 second), and neocortical resection failed to result in seizure freedom.

To provide additional evidence for the accuracy of single-unit classification as excitatory or inhibitory cells using waveform features, we also examined whether the action potentials generated by the single units classified as inhibitory neurons were more strongly phase locked to the LVF rhythm, as compared with the action potentials from single units classified as excitatory neurons.[14] The action potentials generated by human putative excitatory and inhibitory neurons both exhibited phase locking during spontaneous LVF onset seizures (see Fig 1D), but the action potentials generated by putative inhibitory

neurons (n = 94) exhibited stronger phase locking to the LVF activity (20–30Hz) compared to the action potentials recorded from putative excitatory neurons (n = 48; see Fig 1E, Wilcoxon rank sum test, $p < 0.001$), confirming the accuracy of neuron classification using waveform features.[14] To further confirm the accuracy of our assignments, in a subsample of the data we characterized the mean ISI of all units during a baseline (5–40 minute) epoch, a 5-minute preictal-LVF onset epoch, and a 5- to 40-minute postictal epoch. We found that action potentials generated by putative inhibitory neurons (n = 29) exhibited relatively briefer ISIs, as compared to excitatory neurons (n = 91), during the baseline and preictal epochs (Wilcoxon rank sum, $p < 0.016$, Bonferroni corrected; see Fig 1F).

We next examined whether the action potential waveforms of the putative excitatory and inhibitory neurons changed their morphology during the LVF seizure onset epoch. Using the first and second principal components, derived from a principal component analysis of the preictal and LVF onset action potential wave-forms, we computed a single squared Mahalanobis distance value for each single unit. No single-unit action potential morphology exhibited a squared Mahalanobis distance value consistent with a significant change ($p \gg 0.05$). Rather, all action potentials generated by all the units exhibited a squared Mahalanobis distance consistent with very little to no change in waveform morphology during LVF onset (Fig 2D).[25] Because the action potential sorting process reduces the variability of waveform morphology, we also investigated whether the action potential waveform morphology of MUA was altered during LVF seizure onset. We found that MUA waveform morphology also did not change during LVF onset as quantified with the squared Mahalanobis distance ($p > 0.05$; see Fig 2E–G).

Changes in the Firing Rate of Excitatory and Inhibitory Neurons during LVF Seizure Onset

Prior to LVF onset, 7 seizures exhibited a sentinel epileptiform discharge(s). In 2 of these seizures, during the sentinel epileptiform discharge the firing rates of excitatory neurons showed an increase. In 2 other seizures (462sz1, 487_44), the firing rates of both excitatory and inhibitory neurons increased. Raster plots of the SUA during individual seizures revealed that, in a subset of the seizures (TJU-49, 461, 489_30), the firing rate of inhibitory interneurons appeared to increase prior to LVF onset. However, comparing the firing patterns of the putative excitatory and inhibitory neurons during all the spontaneous LVF onset seizures revealed that the firing rate of inhibitory interneurons increased after the start of LVF activity in the mesial temporal SOZ (Figs 3–5; $p < 0.01$). Following this initial increase in inhibitory neuron firing, the firing rate of excitatory neurons increased as well (see Figs 3–5; $p < 0.01$).

We confirmed and quantified these changes in single-unit firing rates in the SOZ prior to and during LVF onset across all the seizures (see Figs 4 and 5). The single-unit analysis was performed after aligning each LFP to LVF onset. Spectral analysis of the aligned LFPs confirmed the accuracy of the alignment (see Fig 4A). Across all the seizures, and for the entire duration that the seizures were analyzed, the firing pattern of excitatory and inhibitory neurons appeared heterogeneous.[24,25] However, a change in excitatory and inhibitory firing rate was evident at the time of LVF onset (see Figs 4 and 5). Prior to LVF onset, inhibitory interneurons in the SOZ did not increase their firing rate ($p = 0.61$), but following LVF onset

an increase in the inhibitory neuron firing rate reached maximum after 3 seconds (n = 40, $p < 0.01$). In the entorhinal cortex, inhibitory cell firing peaked 12.5 seconds after LVF onset (n = 7, $p < 0.01$). By contrast, an increase in the excitatory neuron firing rate was not seen until 18.5 seconds after LVF onset (n = 70, $p < 0.01$). In the amygdala and hippocampus, excitatory cell firing peak6ed 13 seconds after LVF onset (n = 30, $p < 0.01$).

We also examined the changes in excitatory and inhibitory cell firing in sites of seizure spread, particularly in the mesial–temporal lobe contralateral to the SOZ (Figs 6 and 7). We found that during LVF spread to the contra-lateral amygdala and hippocampus, the firing rate of inhibitory interneurons peaked about 2 seconds after the onset of LVF activity in the contralateral microelectrode LFP ($p < 0.01$; see Figs 6 and 7). The firing rate of excitatory neurons in the sites of spread also increased, following the increase in the firing rate of inhibitory interneurons ($p < 0.01$).

Discussion

We studied single- and multiunit firing in LFP recordings during spontaneous LVF onset seizures in patients with mesial–temporal lobe epilepsy and found that single- and multiunit spikes did not change morphology during LVF ictal onset, and that single-unit spike waveforms could be reliably sorted and classified as being generated by putative excitatory and inhibitory neurons. During LVF onset, in the entorhinal cortex, hippocampus, and amygdala SOZ, inhibitory neurons dramatically increased their firing rate prior to an increase in excitatory neuron firing. Contralateral to the SOZ, initially during LVF spread, inhibitory neurons also increased their firing rate. Overall, our findings identify specific changes in the firing of inhibitory and excitatory cells that coincide with the onset of spontaneous LVF seizures in epileptic patients.

Accuracy and Validity of Single-Unit Spike Sorting during Seizure Onset

Using both SUA analysis and MUA analysis approaches, we found that the morphology of action potentials remains unaltered during LVF oscillations in the SOZ and in sites of spread. MUA analysis was necessary for this proof, because SUA analysis may introduce a bias toward excluding action potentials with an altered morphology.[30] It should be noted that our results differ from those obtained using microelectrode arrays implanted in human neocortex, which showed how in the ictal core, single units could not be discriminated during seizures.[32] The disparity is not due to electrode placement, because in our study, the ictal core would encompass the mesial–temporal SOZ and later some of the sites of spread in patients with MTLE (see Fig 6).[29] One reason that SUA analysis could be successfully performed in LFP recordings from the “ictal core” may be that in this previous study unit activity was analyzed during both the ictal onset pattern and the following clonic bursting.[32] In contrast, here we restricted the analysis of neuronal spiking to the LVF onset epoch and found that action potential waveform morphology was stable.[25] Demonstrating this stability was critical for establishing that action potentials from putative excitatory and inhibitory interneurons could be reliably identified during seizure onset.

We used established criteria to discriminate putative excitatory principal neurons from interneurons that are putatively inhibitory on the basis of waveform morphology.[14,33,38,39]

Other approaches to discriminating principal neurons from interneurons have addressed the temporal autocorrelation of the spike train.[21,29] This approach, however, may be inappropriate for ictal epochs due to the atypical neuronal firing patterns. The validity of our spike sorting approach was further supported in that the putative inhibitory neurons were phase locked to the gamma frequency occurring during LVF activity, whereas the putative excitatory neurons were less often phase locked to LVF activity.[14,21] Inhibitory postsynaptic potentials (IPSPs) caused by the release of γ-aminobutyric acid (GABA) from inhibitory interneurons are believed to be the primary generator of gamma rhythms during cognition,[40] and perhaps IPSPs resulting from the phase locked action potentials of inhibitory interneurons also generate the LVF rhythm during seizure onset. We also recognize that the mesial–temporal structures that we sampled with microelectrodes could be damaged in some patients (due to mesial–temporal sclerosis or other lesions) and that this damage could have altered the waveforms of the single-unit spikes. However, prior single-unit studies in patients with epilepsy have shown that putative excitatory and inhibitory units can be reliably distinguished.[41]

Excitatory/Inhibitory Imbalance during LVF Onset in the SOZ

Across all the seizures examined in this study, in the entorhinal cortex onset zone, inhibitory neuron firing dramatically increased at LVF onset, presumably suppressing excitatory neuron firing. Approximately 10 seconds after LVF onset, we observed an increase or rebound of excitatory neuron firing. This pattern of first inhibitory, then excitatory neuron firing during LVF onset in the entorhinal cortex recapitulates the firing pattern of excitatory and inhibitory neurons in some pharmacologically induced seizures in animal models[12–14,42] and in optogenetic studies.[15,16,43] In the present study, in the hippocampus and amygdala SOZ, the LVF onset pattern was also associated with increased inhibitory neuron firing. Following the increase in the inhibitory neuron firing rate, we observed a significant increase in the firing rate of excitatory neurons during LVF onset in the mesial–temporal onset zone. The role of excitatory/inhibitory balance in the hippocampus and amygdala during LVF seizure genesis has been investigated in epileptic rodents in vivo,[22] but not with optogenetic stimulating procedures.[15–17] Our findings in patients with medically refractory focal epilepsy suggest that these structures are involved in seizure genesis.

Excitatory/Inhibitory Imbalance during LVF Spread

We found that inhibitory neuron firing also increased during LVF spread in mesial–temporal lobe structures contra-lateral to the SOZ. Following the increase in inhibitory neuron firing, an increase in excitatory neuron firing was evident. The significance of the increase in inhibitory neuron firing during LVF spread is not yet clear. The inhibitory interneurons in the region of spread were phase locked to the LVF oscillations, suggesting that they may have been intrinsically involved in the generation of the LVF spread. Alternatively, the increase in the firing rate of local inhibitory interneurons in sites of spread could reflect an inhibitory restraint mechanism.[26,35,44] However, the excitatory neurons at these sites were quiescent before and during the LVF activity.

Another interpretation is that LVF activity may not be a seizure onset pattern at all, but may reflect propagation of unseen hypersynchronous onset seizures. LVF onsets are usually

regional, whereas hypersynchronous onsets are usually focal, and the former are associated with a poorer out-come than the latter.[8,9] Most often hypersynchronous seizure onset is associated with mesial–temporal lobe sclerosis, and only 1 of the 9 patients in the study cohort exhibited hippocampal sclerosis on magnetic resonance imaging and pathology. However, in a single seizure recording from a patient in a prior study, a hypersynchronous microseizure was present on microelectrode recordings prior to LVF onset seen in the clinical macroelectrodes,[29] suggesting that some of the LVF onset seizures analyzed in this study may also reflect propagated events.

In the neocortex, it is unclear whether inhibition promotes or suppresses spontaneous neocortical LVF seizure genesis and spread. Calcium imaging of optogenetically kindled neocortical seizures demonstrates that inhibitory parvalbumin and somatostatin interneurons are activated prior to the excitatory neurons in the SOZ.[43] The mechanism by which the specific excitatory/inhibitory imbalance at LVF onset promotes seizure genesis is not yet resolved but may involve depolarizing GABAergic activity[45] or potassium and chloride efflux due to activation of the KCC2 cotransporter.[46,47] It is possible that novel pharmacological interventions could reduce inhibitory interneuron overactivation and thereby prevent seizure evolution.

Conclusions

We have shown in this study that, in patients with epilepsy, spontaneous mesial–temporal LVF onset begins with increased inhibitory neuron firing. Two possible interpretations of this finding are that increased firing of inhibitory neurons could be either (1) directly responsible for LVF ictogenesis or (2) a protective mechanism preceding propagation of a distant focal ictal onset. Further studies employing pharmacological and optogenetic approaches in animal models of epilepsy are required to fully resolve this issue. Another important additional question is whether other seizure onset patterns[7] exhibit similar or distinct patterns of inhibitory/excitatory imbalance.

Data and Software Availability

Some of the raw ictal local field potential recordings are available on the international EEG portal (www.ieeg.org). Some raw and all analyzed data are available on a permanent Zenodo repository (https://www.zenodo.org/record/836286#.WX0Ht9PyuWZ and https://zenodo.org/record/1240532#.WvHDGdPwZBw). MATLAB code used for data analysis is permanently available on GitHub (https://github.com/shennanw/lvf_code).

Acknowledgment

This work was supported by the NIH (R01 NS033310, J.E.) and Commonwealth Universal Research Enhancement program grants (4100077067, 5K23NS094633–02, S.A.W.; 5R01NS084017–05, NS033221, I.F.).

We thank the patients who participated in this study; and M. Leng for statistical assistance.

References

1. Ayala GF, Dichter M, Gumnit RJ. Genesis of epileptic interictal spikes. New knowledge of cortical feedback systems suggests a neurophysiological explanation of brief paroxysms. Brain Res 1973; 52:1–17. [PubMed: 4573428]
2. Trevelyan AJ, Muldoon SF, Merricks EM, et al. The role of inhibition in epileptic networks. J Clin Neurophysiol 2015;32:227–234. [PubMed: 26035675]
3. Avoli M, de Curtis M, Gnatkovsky V, et al. Specific imbalance of excitatory/inhibitory signaling establishes seizure onset pattern in temporal lobe epilepsy. J Neurophysiol 2016;115:3229–3237. [PubMed: 27075542]
4. de Curtis M, Avoli M. Initiation, propagation, and termination of partial (focal) seizures. Cold Spring Harb Perspect Med 2015;5:a022368. [PubMed: 26134843]
5. Spencer SS, Spencer DD. Entorhinal-hippocampal interactions in medial temporal lobe epilepsy. Epilepsia 1994;35:721–727. [PubMed: 8082614]
6. Velasco AL, Wilson CL, Babb TL, Engel J Jr. Functional and anatomic correlates of two frequently observed temporal lobe seizure-onset patterns. Neural Plast 2000;7:49–63. [PubMed: 10709214]
7. Perucca P, Dubeau F, Gotman J. Intracranial electroencephalographic seizure-onset patterns: effect of underlying pathology. Brain 2014;137:183–196. [PubMed: 24176980]
8. Memarian N, Madsen SK, Macey PM, et al. Ictal depth EEG and MRI structural evidence for two different epileptogenic networks in mesial temporal lobe epilepsy. PLoS One 2015;10:e0123588. [PubMed: 25849340]
9. Ogren JA, Bragin A, Wilson CL, et al. Three-dimensional hippocampal atrophy maps distinguish two common temporal lobe seizure-onset patterns. Epilepsia 2009;50:1361–1370. [PubMed: 19054395]
10. Lopantsev V, Avoli M. Participation of GABAA-mediated inhibition in ictallike discharges in the rat entorhinal cortex. J Neurophysiol 1998; 79:352–360. [PubMed: 9425204]
11. Ziburkus J, Cressman JR, Barreto E, Schiff SJ. Interneuron and pyramidal cell interplay during in vitro seizure-like events. J Neurophysiol 2006;95:3948–3954. [PubMed: 16554499]
12. Gnatkovsky V, Librizzi L, Trombin F, de Curtis M. Fast activity at seizure onset is mediated by inhibitory circuits in the entorhinal cortex in vitro. Ann Neurol 2008;64:674–686. [PubMed: 19107991]
13. Uva L, Breschi GL, Gnatkovsky V, et al. Synchronous inhibitory potentials precede seizure-like events in acute models of focal limbic seizures. J Neurosci 2015;35:3048–3055. [PubMed: 25698742]
14. Lévesque M, Herrington R, Hamidi S, Avoli M. Interneurons spark seizure-like activity in the entorhinal cortex. Neurobiol Dis 2016;87: 91–101. [PubMed: 26721318]
15. Shiri Z, Manseau F, Lévesque M, et al. Interneuron activity leads to initiation of low-voltage fast-onset seizures. Ann Neurol 2015;77: 541–546. [PubMed: 25546300]
16. Shiri Z, Manseau F, Lévesque M, et al. Activation of specific neuronal networks leads to different seizure onset types. Ann Neurol 2016;79: 354–365. [PubMed: 26605509]
17. Yekhlef L, Breschi GL, Lagostena L, et al. Selective activation of parvalbumin- or somatostatin-expressing interneurons triggers epileptic seizurelike activity in mouse medial entorhinal cortex. J Neurophysiol 2015;113:1616–1630. [PubMed: 25505119]
18. Bragin A, Engel J Jr, Wilson CL, et al. Electrophysiologic analysis of a chronic seizure model after unilateral hippocampal KA injection. Epilepsia 1999;40:1210–1221. [PubMed: 10487183]
19. Bragin A, Azizyan A, Almajano J, et al. Analysis of chronic seizure onsets after intrahippocampal kainic acid injection in freely moving rats. Epilepsia 2005;46:1592–1598. [PubMed: 16190929]
20. Lévesque M, Salami P, Gotman J, Avoli M. Two seizure-onset types reveal specific patterns of high-frequency oscillations in a model of temporal lobe epilepsy. J Neurosci 2012;32:13264–13272. [PubMed: 22993442]
21. Grasse DW, Karunakaran S, Moxon KA. Neuronal synchrony and the transition to spontaneous seizures. Exp Neurol 2013;248:72–84. [PubMed: 23707218]

22. Karunakaran S, Grasse DW, Moxon KA. Role of CA3 theta-modulated interneurons during the transition to spontaneous seizures. Exp Neurol 2016;283:341–352. [PubMed: 27353968]
23. de Curtis M, Gnatkovsky V. Reevaluating the mechanisms of focal ictogenesis: the role of low-voltage fast activity. Epilepsia 2009;50: 2514–2525. [PubMed: 19674056]
24. Truccolo W, Donoghue JA, Hochberg LR, et al. Single-neuron dynamics in human focal epilepsy. Nat Neurosci 2011;14:635–641. [PubMed: 21441925]
25. Lambrecq V, Lehongre K, Adam C, et al. Single-unit activities during the transition to seizures in deep mesial structures. Ann Neurol 2017; 82:1022–1028. [PubMed: 29205475]
26. Schevon CA, Weiss SA, McKhann G Jr, et al. Evidence of an inhibitory restraint of seizure activity in humans. Nat Commun 2012;3: 1060. [PubMed: 22968706]
27. Fried I, Wilson CL, Maidment NT, et al. Cerebral microdialysis combined with single-neuron and electroencephalographic recording in neurosurgical patients. Technical note. J Neurosurg 1999;91: 697–705. [PubMed: 10507396]
28. Staba RJ, Wilson CL, Bragin A, et al. Quantitative analysis of high-frequency oscillations (80–500 Hz) recorded in human epileptic hippocampus and entorhinal cortex. J Neurophysiol 2002;88: 1743–1752. [PubMed: 12364503]
29. Weiss SA, Alvarado-Rojas C, Bragin A, et al. Ictal onset patterns of local field potentials, high frequency oscillations, and unit activity in human mesial temporal lobe epilepsy. Epilepsia 2016;57:111–121. [PubMed: 26611159]
30. Quiroga RQ, Nadasdy Z, Ben-Shaul Y. Unsupervised spike detection and sorting with wavelets and superparamagnetic clustering. Neural Comput 2004;16:1661–1687. [PubMed: 15228749]
31. Hill DN, Mehta SB, Kleinfeld D. Quality metrics to accompany spike sorting of extracellular signals. J Neurosci 2011;31:8699–8705. [PubMed: 21677152]
32. Merricks EM, Smith EH, McKhann GM, et al. Single unit action potentials in humans and the effect of seizure activity. Brain 2015; 138:2891–2906. [PubMed: 26187332]
33. Csicsvari J, Hirase H, Czurko A, Buzsáki G. Reliability and state dependence of pyramidal cell–interneuron synapses in the hippo-campus: an ensemble approach in the behaving rat. Neuron 1998; 21:179–189. [PubMed: 9697862]
34. Nadasdy Z, Nguyen TP, Török Á, et al. Context-dependent spatially periodic activity in the human entorhinal cortex. Proc Natl Acad Sci U S A 2017;114:E3516–E3525. [PubMed: 28396399]
35. Weiss SA, Banks GP, McKhann GM Jr, et al. Ictal high frequency oscillations distinguish two types of seizure territories in humans. Brain 2013;136:3796–3808. [PubMed: 24176977]
36. Fisher NI. Statistical analysis of circular data. Cambridge, UK: Cambridge University Press, 1993.
37. Sakata S, Harris KD. Laminar structure of spontaneous and sensory-evoked population activity in auditory cortex. Neuron 2009; 64:404–418. [PubMed: 19914188]
38. Le Van Quyen M, Bragin A, Staba R, et al. Cell type-specific firing during ripple oscillations in the hippocampal formation of humans. J Neurosci 2008;28:6104–6110. [PubMed: 18550752]
39. Viskontas IV, Ekstrom AD, Wilson CL, Fried I. Characterizing inter-neuron and pyramidal cells in the human medial temporal lobe in vivo using extracellular recordings. Hippocampus 2007;17:49–57. [PubMed: 17143903]
40. Buzsáki G, Wang XJ. Mechanisms of gamma oscillations. Annu Rev Neurosci 2012;35:203–225. [PubMed: 22443509]
41. Ison MJ, Mormann F, Cerf M, et al. Selectivity of pyramidal cells and interneurons in the human medial temporal lobe. J Neurophysiol 2011;106:1713–1721. [PubMed: 21715671]
42. Trombin F, Gnatkovsky V, de Curtis M. Changes in action potential features during focal seizure discharges in the entorhinal cortex of the in vitro isolated guinea pig brain. J Neurophysiol 2011;106: 1411–1423. [PubMed: 21676935]
43. Khoshkhoo S, Vogt D, Sohal VS. Dynamic, cell-type-specific roles for GABAergic interneurons in a mouse model of optogenetically inducible seizures. Neuron 2017;93:291–298. [PubMed: 28041880]
44. Weiss SA, Lemesiou A, Connors R, et al. Seizure localization using ictal phase-locked high gamma: a retrospective surgical outcome study. Neurology 2015;84:2320–2328. [PubMed: 25972493]

45. Wang Y, Xu C, Xu Z, et al. Depolarized GABAergic signaling in subicular microcircuits mediates generalized seizure in temporal lobe epilepsy. Neuron 2017;95:92.e5–105.e5. [PubMed: 28648501]

46. Hamidi S, Avoli M. KCC2 function modulates in vitro ictogenesis. Neurobiol Dis 2015;79:51–58. [PubMed: 25926348]

47. Di Cristo G, Awad PN, Hamidi S, Avoli M. KCC2, epileptiform synchronization, and epileptic disorders. Prog Neurobiol 2018; 162:1–16. [PubMed: 29197650]

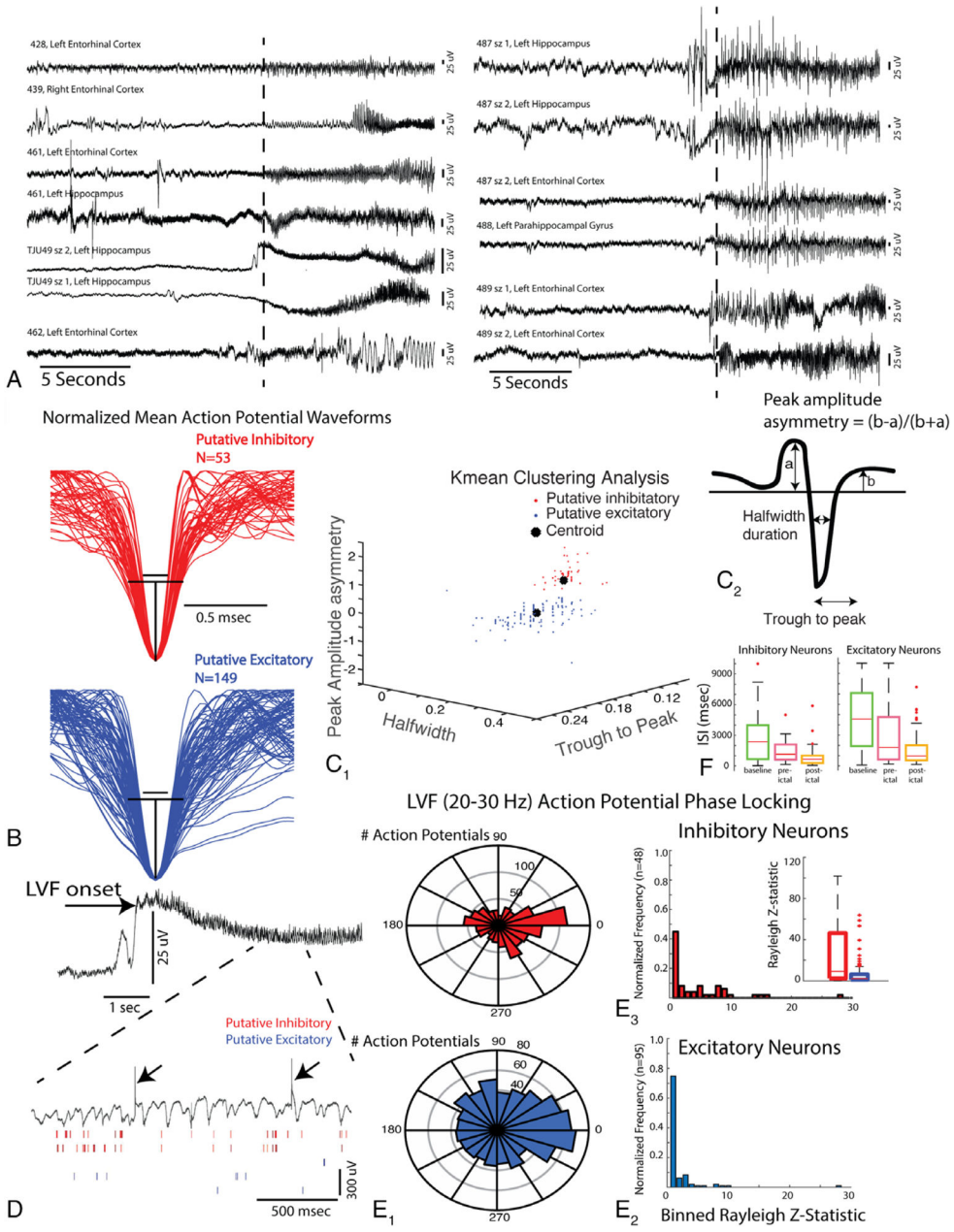

FIGURE 1:

The isolation and characterization of single units in 200 microelectrodes. (A) Local field potential (LFP) recordings of low-voltage fast (LVF) onset seizures. The vertical dashed lines indicate the time of LVF onset determined by spectrographic analysis. sz = seizure. (B) Mean normalized waveforms of putative inhibitory and excitatory neurons isolated from microelectrodes during spontaneous LVF seizures in patients. Black lines illustrate an estimation of the half width of the inhibitory neuron action potentials (top), projected on to the excitatory neuron action potentials (bottom). (C_1) Three-dimensional plot of the extracted features shown in C_2: peak amplitude asymmetry, trough to peak, and half width used to differentiate excitatory and inhibitory neurons on the basis of K-means clustering.

(D) LFP recording of an LVF seizure (top). Note that during the LVF activity (bottom, expanded), the action potentials of inhibitory interneurons are more strongly phase locked to the LVF oscillation. Arrows indicate transient artifacts (bottom). (E_1) Circular histograms of the preferred phase angle of inhibitory interneuron action potentials (red, top) and excitatory neuron action potentials (blue, bottom) with respect to LVF oscillations at 20 to 30Hz (right). (E_2) Normalized histogram of the proportion of units exhibiting an elevated Rayleigh Z statistic (ie, index of phase locking strength). (E_3) Box plot of phase locking strength for the inhibitory and excitatory neurons. (F) Box plot of the inhibitory and excitatory mean interspike interval (ISI) during the baseline, preictal, and postictal epochs.

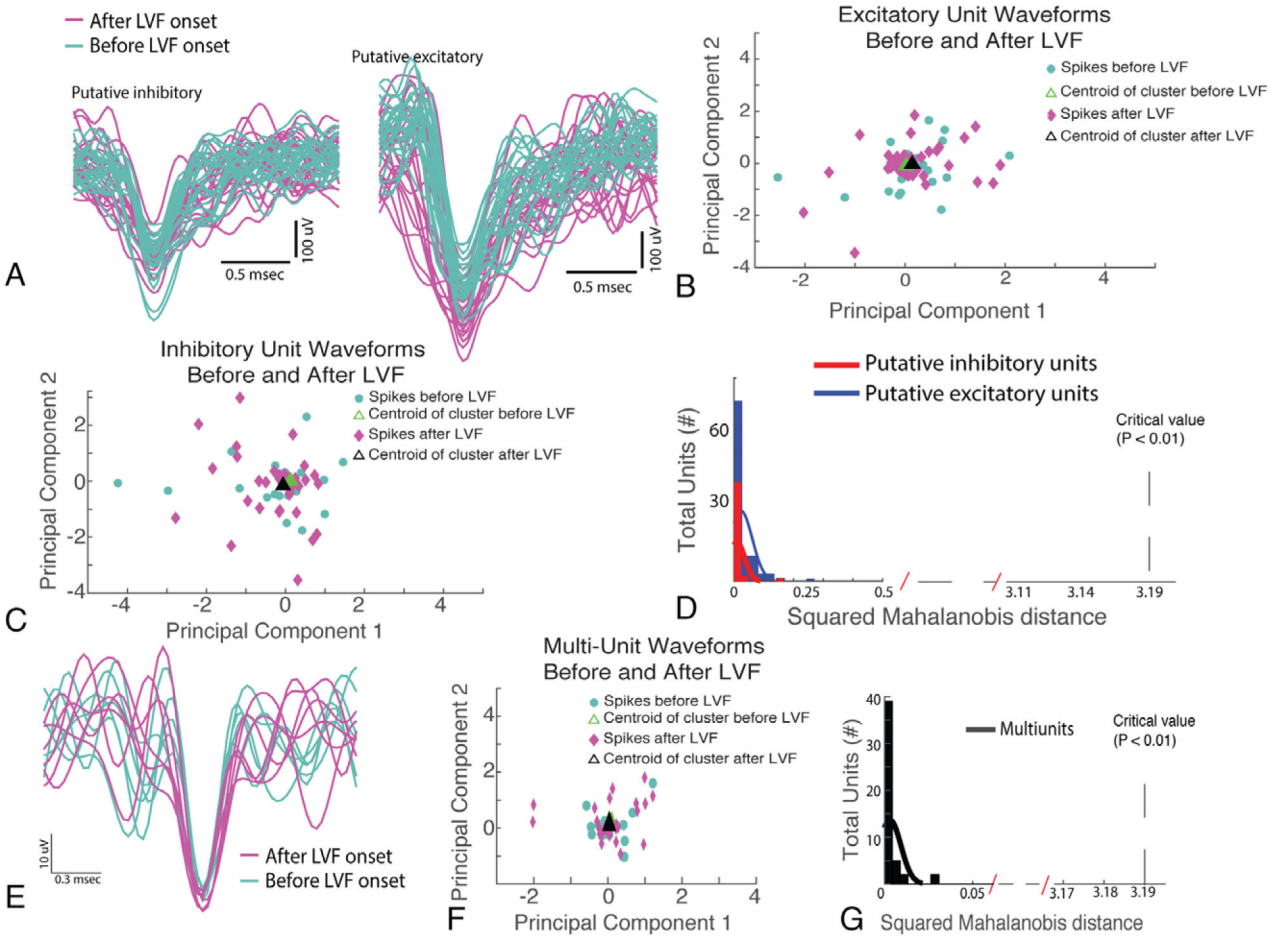

FIGURE 2:

The waveforms of excitatory and inhibitory units remain stable and are unaltered during low-voltage fast (LVF) activity. (A) Examples of inhibitory neuron (left) and excitatory neuron (right) waveforms before (cyan) and after LVF onset (magenta). (B, C) Principal component analysis (PCA) of all the spike waveforms for an excitatory and an inhibitory neuron before (cyan) and after LVF onset (magenta). (D) Histogram of the squared Mahalanobis distance between the centroid of spike clusters in the PCA analysis prior to LVF onset and after LVF onset for all excitatory (blue) and inhibitory (red) neurons recorded in the study. The squared Mahalanobis distance did not meet statistical significance for a change in waveform shape during LVF onset.(E) Representative example of spike waveforms derived using multiunit analysis before (cyan) and after LVF onset (magenta).(F) PCA analysis for the representative multiunit spike waveforms. (G) Histogram of the squared Mahalanobis distance for the multiunit waveforms for >50 distinct local field potential recordings.

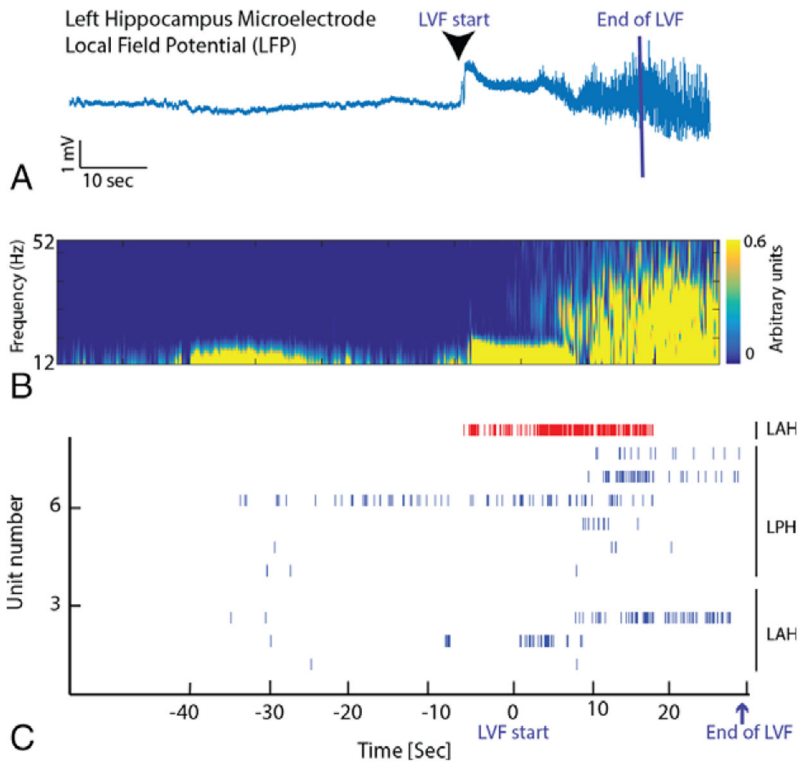

FIGURE 3:

Low-voltage fast (LVF) onset is accompanied by an increase in the firing rate of an inhibitory interneuron followed by a rebound in the firing rate of excitatory neurons. (A) Aligned LFP recorded from a microelectrode in the left hippocampus in patient TJU049 indicating the beginning and end of the LVF onset. LVF onset ended when sharply contoured ictal discharges dominated the LVF activity, and LVF onset ended at different times for each microelectrode recording. (B) Corresponding spectrogram of the increase in the power in faster frequencies during LVF onset. (C) Raster plot of spiking activity of excitatory (blue) and inhibitory neurons (red) prior to and during LVF onset. Note that the raster plot is not aligned with panels A and B, and LVF onset ended at different times for each microelectrode recording. LAH = left anterior hippocampus; LPH = left posterior hippocampus.

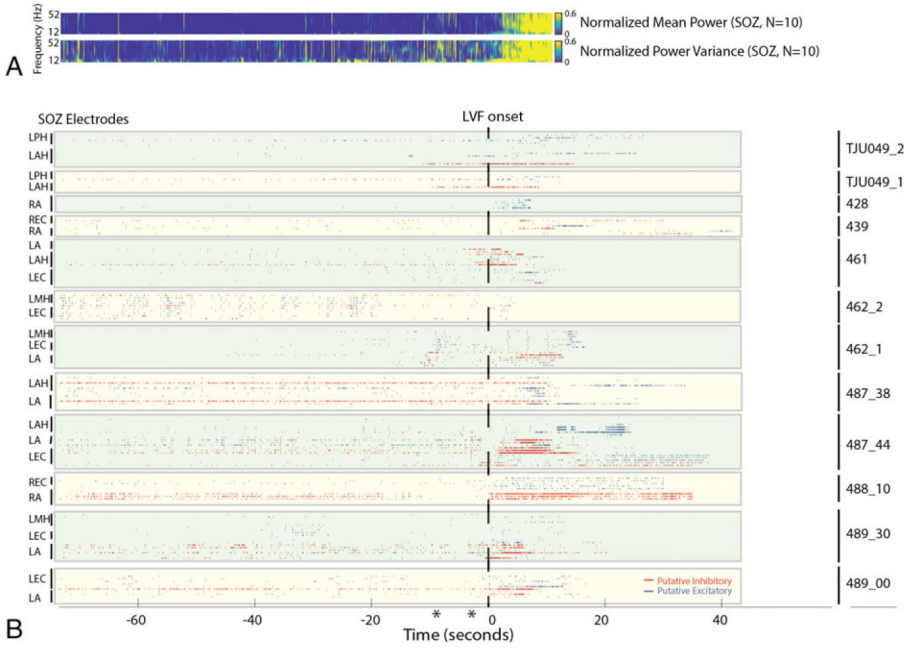

FIGURE 4:

Across all seizures, excitatory and inhibitory neuron firing is heterogeneous, but changes in excitatory and inhibitory balance are evident at the start of low-voltage fast (LVF) seizures in the seizure onset zone (SOZ). (A) Time–frequency plot of the mean normalized power (top) and variance (bottom) prior to and during LVF onset in the local field potential of the SOZ across seizures. (B) Aligned raster plot of 140 units (8 patients, 11 seizures). The seizures are aligned to the onset of LVF activity (*dashed vertical line*). Note that LVF onset ended at different times for each microelectrode recording. Excitatory neurons in the SOZ are shown in blue; inhibitory neurons in the SOZ are shown in red. Asterisks indicates the time of preictal discharges during the seizures 462_1 and 487_44. LA = left amygdala; LAH = left anterior hippocampus; LEC = left entorhinal cortex; LMH = left middle hippocampus; LPH = left posterior hippocampus; RA = right amygdala; REC = right entorhinal cortex.

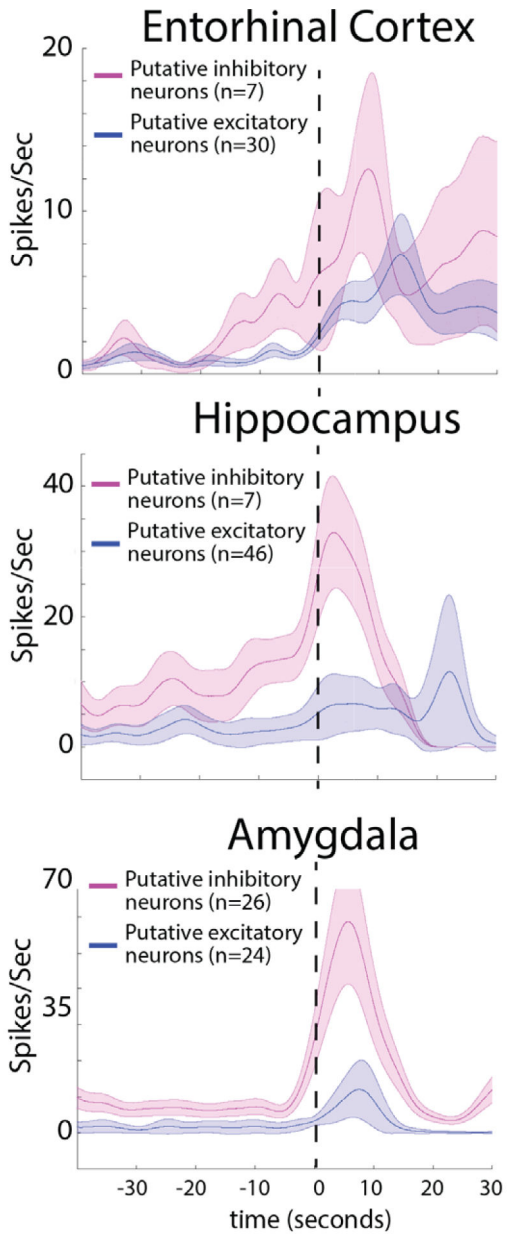

FIGURE 5:

In the seizure onset zone (SOZ), the firing rate of inhibitory neurons increases during low-voltage fast (LVF) onset and is followed by an increase in the firing rate of excitatory neurons. Comparison is shown of the mean action potential firing rate after smoothing using a Gaussian kernel for excitatory (blue) and inhibitory (red) neurons before and during LVF onset in the entorhinal cortex, hippocampus, and amygdala SOZ. Shaded areas represent the standard error of the mean.

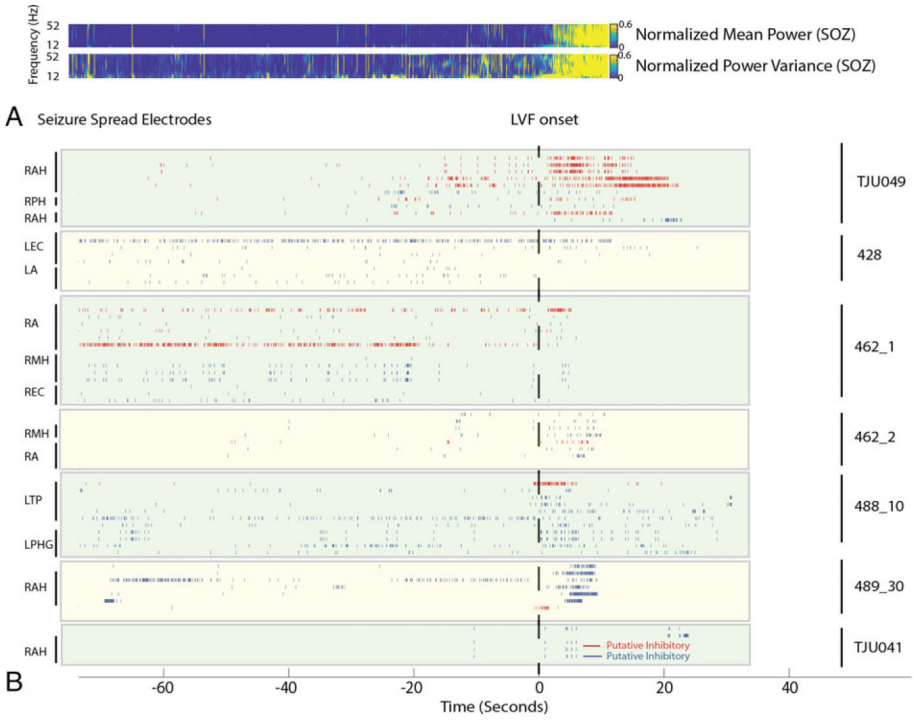

FIGURE 6:

Across all seizures, an increase in the firing rate of inhibitory interneurons occurs at sites of low-voltage fast (LVF) spread. (A) Time–frequency plot of the mean normalized power (top) and variance (bottom) prior to and during LVF onset in the local field potential of the seizure onset zone (SOZ) across seizures. (B) Aligned raster plot of 62 units (7 patients, 7 seizures). The seizures are aligned to the onset of LVF activity (*dashed vertical line*). Excitatory neurons in the non-SOZ are shown in blue; inhibitory neurons in the NSOZ are shown in red. Note that LVF onset ended at different times for each microelectrode recording. LA = left amygdala; LEC = left entorhinal cortex; LPHG = left parahippocampal gyrus; RA = right amygdala; RAH = right anterior hippocampus; REC = right entorhinal cortex; RMH = right middle hippocampus; RPH = right posterior hippocampus.

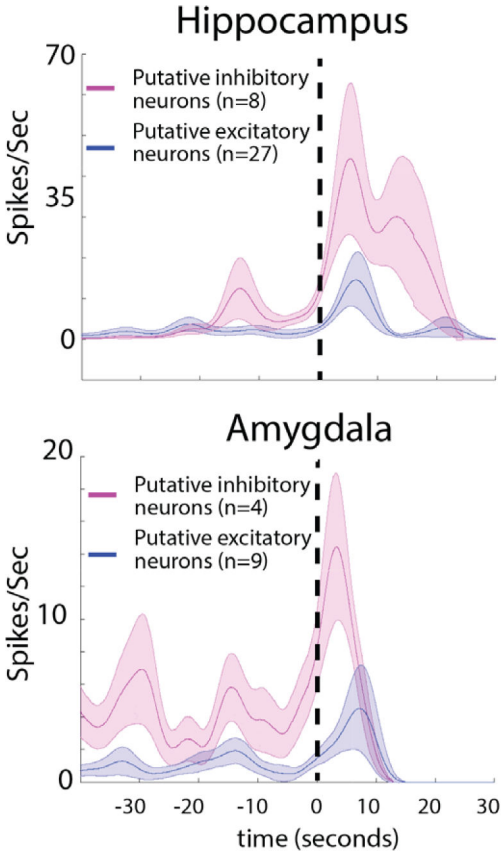

FIGURE 7:

Contralateral to the seizure onset zone, the firing rate of inhibitory neurons also increases during low-voltage fast (LVF) activity prior to an increase in the firing rate of excitatory neurons. Comparison is shown of the mean action potential firing rate after smoothing using a Gaussian kernel for excitatory (blue) and inhibitory (red) neurons prior to and during LVF onset in the amygdala and hippocampus contralateral to the seizure onset zone. Shaded areas represent the standard error of the mean.

TABLE 1.

Patient Characteristics

Patient/Age, yr/Gender	Epilepsy Duration/Risk Factors/Scalp EEG	MRI	PET Hypometabolic	iEEG IED	iEEG SOZ	Surgery	Pathology	Outcome	Single Units Isolated, n
TJ041/20/M	10 yr/none/right temporal	Right temporal subcortical T2	Right temporal	Right mesial neocortical temporal	Right mesial neocortical temporal	Right ATL	Gliosis	Engel III at 6 yr	ex = 5, in = 0
TJ049/39/F	3 yr/none/left temporal	Scattered T2 signal abnormality	Normal	Left and right mesial temporal	Left mesial temporal	Left ATL	Gliosis	Engel Ia at 5 yr	sz 1: ex = 3, in = 2; sz 2: ex= 11, in = 8
428/44/M	4 yr/none/left temporal	Left MTS	Left temporal	Left mesial temporal	Left mesial temporal	Left ATL	Gliosis	Engel Ib at 4 yr	ex= 11, in = 0
439/48/F	18 yr/none/left temporal	Normal	Normal	Left and right mesial temporal	Right mesial temporal	Right ATL	FCD 1c	Engel Ia at 4 yr	ex = 4, in = 3
461/21/M	4 yr/none/left temporal	FCD and subependymal nodule	Left temporal	Left mesial and lateral mesial temporal	Left mesial temporal	Left ATL	Cortical and hippocampal tubers	Lost to follow-up	ex = 9, in = 7
462/27/M	19yr/TBI/left and right temporal	Normal	Left temporal	Left mesial neocortical temporal	Left mesial neocortical temporal	Left Temporal hippocampal sparing	Gliosis	Engel III at 1 yr	sz 1: ex = 21, in = 5; sz 2: ex = 13, in = 8
487/33/F	2.5 yr/none/left temporal	Normal	Left temporal	Left mesial temporal	Left mesial temporal	RNS	N/A	N/A	sz 1: ex = 10, in = 2; sz 2: ex = 15, in = 7
488/38/M	28 yr/perinatal disttess, TBI/left temporal	Right parietal and frontal gyrus atrophy	Right parietal and frontal gyrus	Right posterior temporal parietal	Right mesial temporal frontal	Right ATL	Hippocampal sclerosis	Engel I at 3 mo	ex = 16, in = 4
489/46/F	30 yr/possible TBI/left temporal	T2 signal left amygdala, temporal pole	Left temporal	Left and right mesial temporal	Left and right mesial temporal	RNS	N/A	N/A	sz 1: ex = 21, in = 5; sz 2: ex = 7, in = 2

ATL = anterior temporal lobectomy; EEG = electroencephalography; ex = excitatory neurons; F = female; FCD = focal cortical dysplasia; IED = interictal epileptiform discharge; iEEG = intracranial EEG; in = inhibitory neurons; M = male; MRI = magnetic resonance imaging; MTS = mesial temporal lobe sclerosis; N/A = not available; PET = positron emission tomography; RNS = responsive nerve stimulator; SOZ = seizure onset zone; sz = seizure; TBI = traumatic brain injury.